Journal of Medicinal Chemistry

pubs.acs.org/jmc

Article

Identification and Validation of an Inhibitor of the Protein Kinases PIM and DYRK

Gyula Bencze,[⊥] Prabhadevi Venkataramani,[⊥] Elad Elkayam, Keith D. Rivera, Ankur Garg, Istvan Szabadakai, Laszlo Orfi, Leemor Joshua-Tor, Darryl J. Pappin, and Nicholas K. Tonks*

Cite This: J. Med. Chem. 2026, 69, 7920−7932

Read Online

ACCESS | Metrics & More | Article Recommendations | Supporting Information

ABSTRACT: Fermented wheat germ extract (FWGE), a nutraceutical with reported anticancer properties, contains numerous biologically active molecules, but its therapeutic constituents remain unclear. In this study, we identify and characterize a novel small-molecule protein kinase inhibitor isolated from FWGE, designated F10V6W0. Through preparative high-performance liquid chromatography and structural elucidation via X-ray crystallography, this compound was revealed to be a unique benzothiazole. Kinase profiling demonstrated its selectivity toward PIM and DYRK protein kinase families. A chemically synthesized version (CSH-4044), mirrored the activity of the natural product, confirming structural integrity and biological equivalence. We determined the cocrystal structure of CSH-4044 bound to PIM1, revealing ATP-competitive binding and critical hydrophobic and hydrogen-bonding interactions. Functionally, CSH-4044 suppressed PIM3-driven BAD phosphorylation in pancreatic cancer cells and reduced DYRK1A-mediated Tau phosphorylation in neuronal cells. Our findings position CSH-4044 as a promising lead for targeting PIM and DYRK kinase families and highlight FWGE as a potential therapeutic compounds.

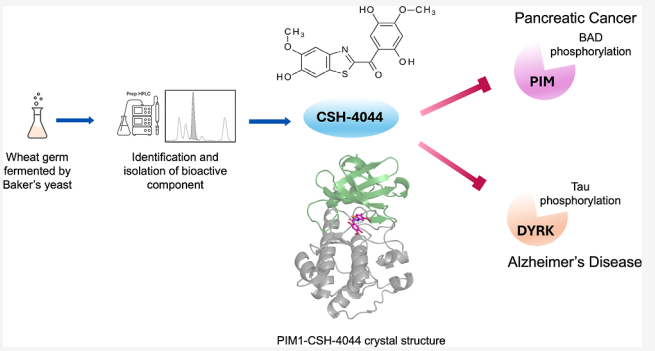

INTRODUCTION

In recent years, nutraceuticals have been gaining importance as therapeutic agents for cancer due to their low toxicity and promising effects in patients.[1] One such nutraceutical, a natural derivative of fermented wheat germ extract (FWGE), has been used to treat cancer patients undergoing chemotherapy or radiotherapy in Eastern European countries.[2] It has been reported to be effective against different cancer types, including lung, colon, prostate, and breast cancer.[3] The antiproliferative activity of FWGE has also been studied in various animal models and cancer cell-lines and is shown to trigger tumor cell-death in a dose-dependent manner.[4,5] One such study demonstrated that FWGE in combination with cisplatin had antiproliferative effects and potentiated cisplatin-induced apoptosis in ovarian cancer.[4] In addition, some studies have also investigated its potential to inhibit cell migration and invasion in oral squamous cell carcinoma.[5]

The production process of FWGE involves fermentation of wheat germ by *Saccharomyces cerevisiae* followed by liquid separation, drying, and granulation.[6] Like other nutraceuticals, FWGE likely contains a wide array of different molecules. Thus, exploiting its full potential will require a more precise definition of the active core components of the mixture and the biochemical characterization of its mechanism of action. Recent studies indicate that two quinones, 2-methoxy benzoquinone and 2,6-dimethoxy benzoquinone, might contribute to the biological activity of FWGE.[7] In this study, in which we sought to identify additional active components of the extract, we generated different fractions of FWGE using preparative high performance liquid chromatography (HPLC). Starting from subfraction A250, we purified and crystallized a novel protein kinase inhibitor. We also established a synthetic route to generate sufficient quantities for structure−activity relationship (SAR) studies. The synthetic form of the inhibitor is designated as CSH-4044.

In this study, we identify and characterize CSH-4044, a unique nutraceutical-derived small molecule that functions as an ATP-competitive inhibitor of PIMs and DYRKs, belonging to the CAMK and CMGC family of kinases, respectively.[8,9] We determined its structure by X-ray crystallography, established its mode of binding to PIM1, and confirmed its activity through both natural product isolation and synthetic reproduction. Functionally, we demonstrate that CSH-4044

Received: November 6, 2025
Revised: February 19, 2026
Accepted: March 3, 2026
Published: March 18, 2026

Table 1. Inhibitory Activity of Different Subfractions of A250 against Protein Kinases[a,b]

	A250-c7		2ND		EP-DIPE		EP-NDS		NDS-510		NDS-1015		NDS-1520		NDS-2025	
	100 μg/ml	10 μg/ml	100 μg/ml	10 μg/ml	100 μg/ml	10 μg/ml	100 μg/ml	10 μg/ml	100 μg/ml	10 μg/ml	100 μg/ml	10 μg/ml	100 μg/ml	10 μg/ml	100 μg/ml	10 μg/ml
P38aMAPK	112	101	97	110	112	128	139	111	104	102	125	104	123	101	157	118
PRAK	85	118	14	110	69	107	71	93	92	107	29	96	42	76	6	62
DAPK1	73	86	41	98	26	87	42	88	81	105	34	80	29	88	9	42
CHK1	102	96	97	99	88	100	144	115	92	84	86	94	120	92	199	148
GSK3b	44	96	84	94	26	89	12	80	71	94	12	72	5	54	3	24
CK2	16	70	67	100	8	69	6	40	23	80	6	14	8	42	11	38
DYRK1A	11	59	17	69	4	31	4	12	12	80	1	3	6	47	0	6
DYRK2	11	49	27	89	1	13	3	15	41	73	2	21	1	18	-1	1
DYRK3	41	81	17	87	12	47	30	47	69	82	4	50	6	48	5	9
PIM1	19	72	23	54	7	45	8	42	41	78	7	35	10	40	1	7
PIM3	13	40	28	91	9	15	6	16	33	82	7	16	5	19	8	5
SRPK1	33	59	16	60	31	72	11	56	37	63	2	33	7	50	5	33
CLK2	32	72	16	87	9	68	10	59	39	77	7	52	8	59	0	10
BTK	41	83	13	38	31	78	23	77	50	84	22	51	20	59	9	40

[a]The subfraction with the highest inhibitory activity primarily targeted PIMs and DYRKs even after dilution. [b](% of residual activity of the kinases, measured in duplicates), the heat map color scale ranges from 0 to 20; values > 20 are capped at the maximum color.

reduces the level of phosphorylation of BAD in pancreatic cancer cells and decreases Tau phosphorylation in neuronal cells, thereby validating its kinase inhibitory activity in two disease models. Our findings highlight FWGE's structurally novel bioactive compounds and establish CSH-4044 as a promising lead scaffold for therapeutic development against PIM- and DYRK-driven pathologies.

RESULTS

Enrichment of Active Fractions from Fermented Wheat Germ Extract

In a previous study from our lab, we isolated Fraction A250 through bioassay-guided fractionation and alcohol extraction from FWGE.[10] Although A250 constituted only 3% of FWGE by mass, it shows antiproliferative activity against different cancer cell lines.[10] Liquid−liquid extraction of Fraction A250 with ethyl acetate yields two distinct subfractions: a hydrophilic aqueous phase (A251) and a lipophilic organic phase (A252). HPLC confirmed that flavonoid glycosides partitioned into A251, whereas dimethoxy benzoquinone (DMBQ) and other components were enriched in A252 (Figure S1A,B). To determine the role of DMBQ, Fraction A252 was treated with ascorbic acid (ASC) in methanol to reduce DMBQ to 2,6-dimethoxyhydroquinone (DMHQ), allowing separation by HPLC (Figure S1C). Although the DMBQ-depleted material (Fraction A252-EP) showed reduced in vitro activity compared with A252, the persistent cytotoxicity of this still-complex fraction suggests the presence of additional, unidentified bioactive components (Table 1).

Kinase Selectivity Profiling of A250-Derived Fractions

As part of the optimized extraction and purification workflow (Figure 1A), we concentrated the small-molecule content of FWGE into Fraction A250 with liquid and solid phase extraction (SPE) methods.

Despite its low abundance, Fraction A250 retained nearly all of the cytotoxic activity observed in crude FWGE. To assess their potential to inhibit protein kinase targets, Fraction A250 and its subfractions, including the hydrophilic A251 and the lipophilic A252, were screened at 100 and 10 μg/mL concentration against a 138-kinase panel (the International Centre for Kinase Profiling, University of Dundee). Initial analysis revealed that whereas A250 exhibited inhibitory activity against several kinases, most of the inhibitory effects localized to Fraction A252, the ethyl acetate-soluble fraction enriched in lipophilic small molecules.

Subsequent fractionation and kinase profiling of A252-derived subfractions led to the identification of a concentrated fraction (NDS-2025) with a highly selective inhibitory profile, primarily targeting the PIM and DYRK families of kinases (Table 1). These findings suggest that the biologically active compound in FWGE may represent a novel and selective chemical scaffold for kinase inhibition, as no such activity has previously been attributed to wheat germ. Due to the pronounced kinase-inhibitory profile of NDS-2025 in a 138-kinase panel screen, especially against PIM3 and DYRK2, larger quantities of A250 were processed for milligram-scale isolation of individual compounds. A combination of preparative-scale, normal-phase flash chromatography, reversed-phase HPLC, and MS-coupled analytical HPLC was employed to isolate purified components from freeze-dried FWGE, yielding subfractions 2025A, B, and C (Figure 1B,C). Among the three subfractions (2025-A, 2025-B, and 2025-C) isolated from NDS-2025, 2025-A demonstrated the lowest IC_{50} values against both PIM3 and DYRK2 (Figure 1D).

Preparative Isolation of Active Subfractions

We used mass spectrometry to determine the most abundant components of fraction 2025-A. Two ions were detected at m/z 348 and m/z 403. A combination of normal phase flash chromatography, reverse-phase HPLC, and MS-coupled analytical HPLC was employed to isolate the detected components into fraction V10 (Figure 2A). Further analysis of this fraction under alternative chromatographic conditions separated the identified components into two distinct peaks (Figure 2B). The activities of the collected fractions (F10V6 and F10V10) and the rest of the run combined (F10VM) were tested against PIM3, and we found that F10V6 showed markedly higher kinase-inhibitory activity (Figure 2C).

Although Fraction F10V6 mainly contained the component with 347 Da molecule weight, mass spectrometric analysis indicated the presence of a minor amount of the second

https://doi.org/10.1021/acs.jmedchem.5c03226
J. Med. Chem. 2026, 69, 7920−7932

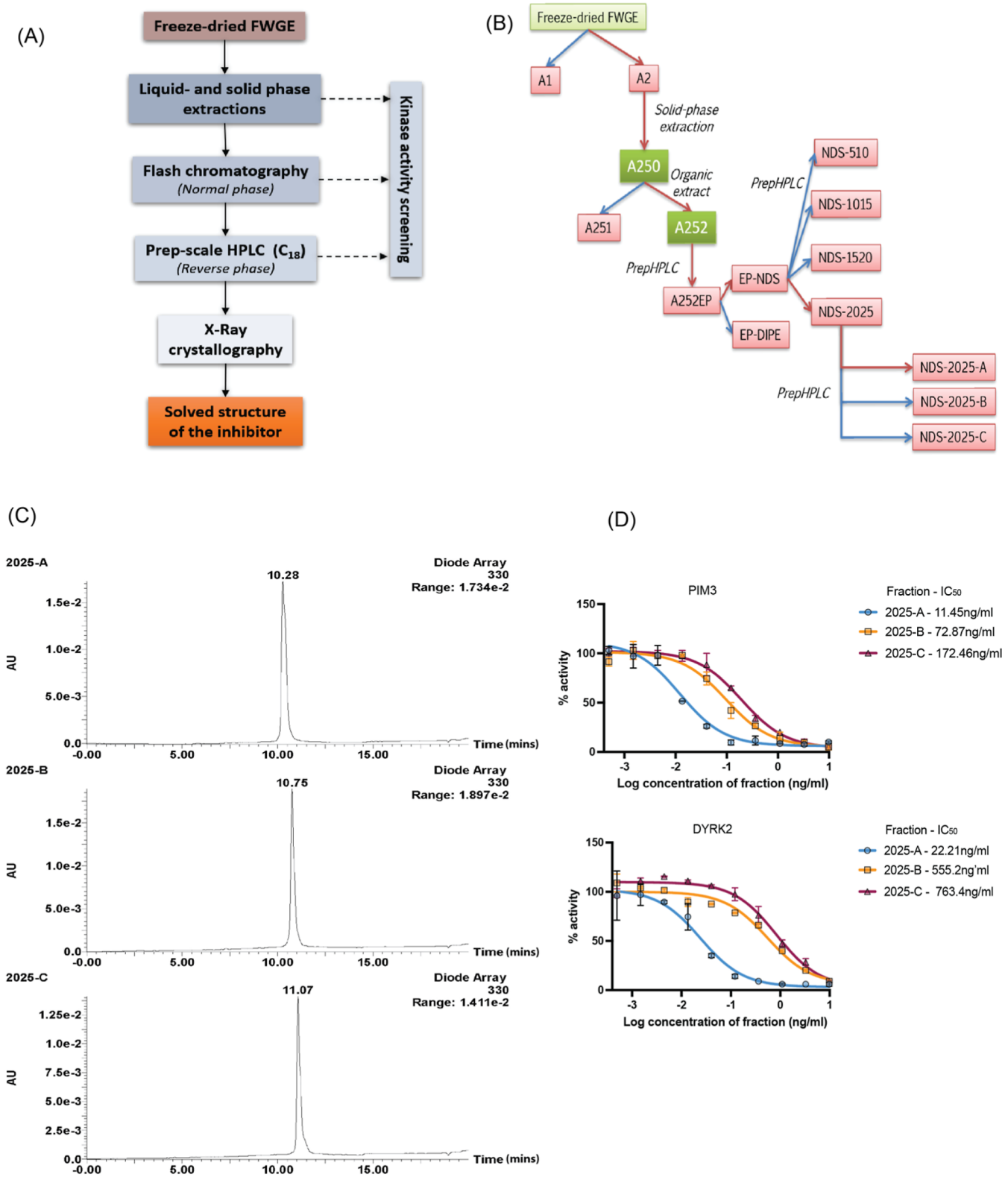

Figure 1. Kinase selectivity profiling of A250-derived fractions, (A) extraction and purification workflow for the isolation of the kinase inhibitor component from freeze-dried FWGE. (B) Flowchart outlining the steps involved in the isolation of fractions from FWGE with the highest activity and (C) HPLC-UV chromatogram (A330) of the fractions −2025 A, 2025 B, and 2025 C. (D) Inhibitory effect of 2025 A, B, and C fractions on PIM3 and DYRK2 kinases (n = 3; biological repeats).

compound. This impurity was removed by washing the sample with di-isopropyl ether. The isolated and purified compound was designated F10V6W0, and its selectivity at 1 μM concentration was assayed against a 138-kinase panel. F10V6W0 was found to inhibit PIMs and DYRKs (Figure 2D, Table S1). To characterize F10V6W0, molecular weight and fragmentation data were obtained using electron ionization mass spectrometry (EI-MS) (Figure S1D). As expected, the

https://doi.org/10.1021/acs.jmedchem.5c03226
J. Med. Chem. 2026, 69, 7920−7932

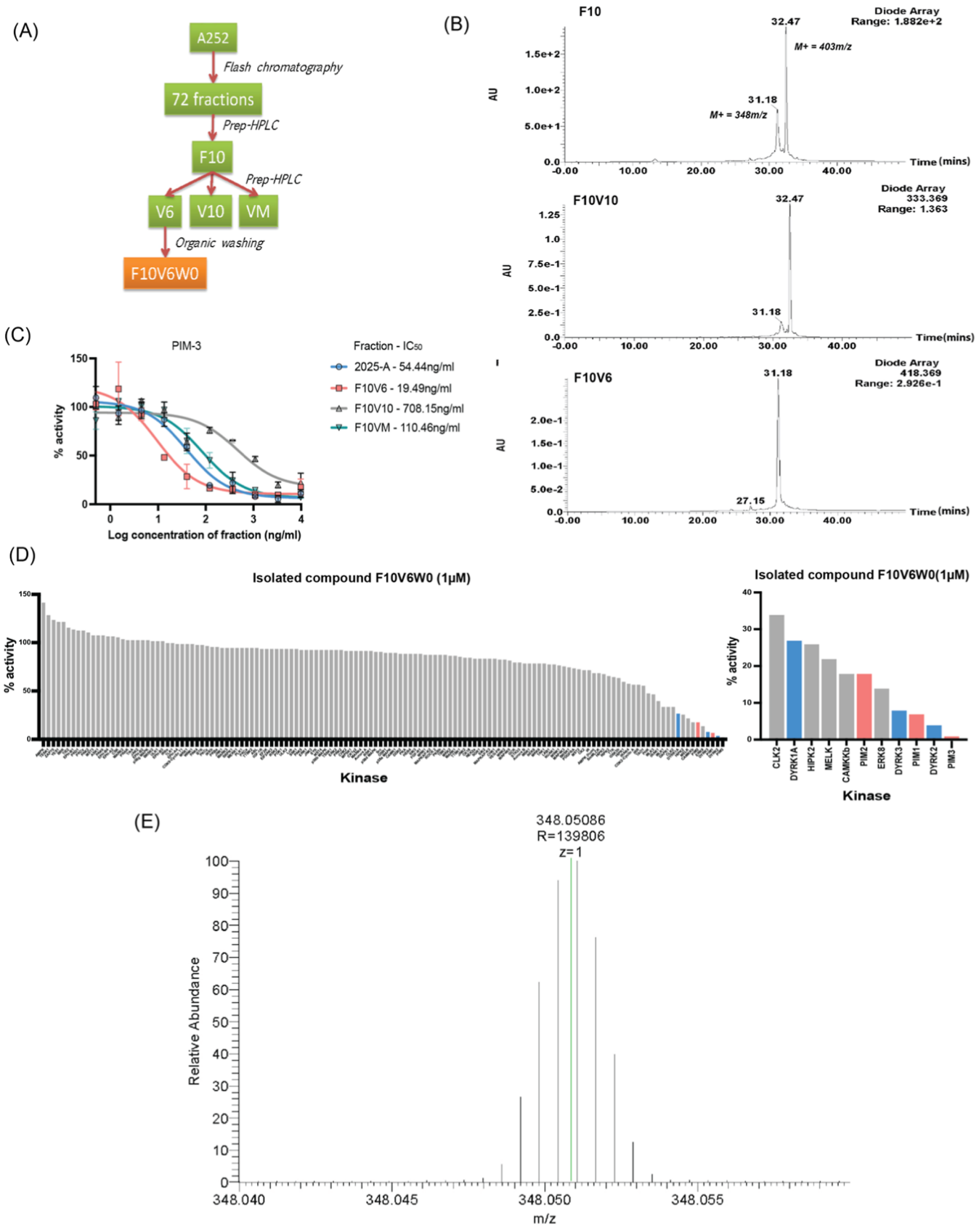

Figure 2. Preparative isolation of the different fractions, (A) flowchart outlining the isolation of F10V6 from FWGE. (B) F10V6 contains the component eluted at 31.18 min (top) and appeared as a single peak on the chromatogram recorded at 415 nm (bottom), whereas F10V10 mainly contains the component that was eluted at 32.47 min and was most abundant at 335 nm. (Middle) (C) IC_{50} of 2025-A and its isolated components against PIM3 (n = 2; biological repeats) and (D) waterfall plot of the kinase selectivity panel (left) for the isolated compound F10V6W0 (1 μM).

https://doi.org/10.1021/acs.jmedchem.5c03226
J. Med. Chem. 2026, 69, 7920−7932

Figure 2. continued

The PIM and DYRK kinases are labeled in red and blue, respectively, (A) selection of most-inhibited kinases is shown on the right. (E) Orbitrap Q-TOF data of isolated kinase inhibitor F10V6W0.

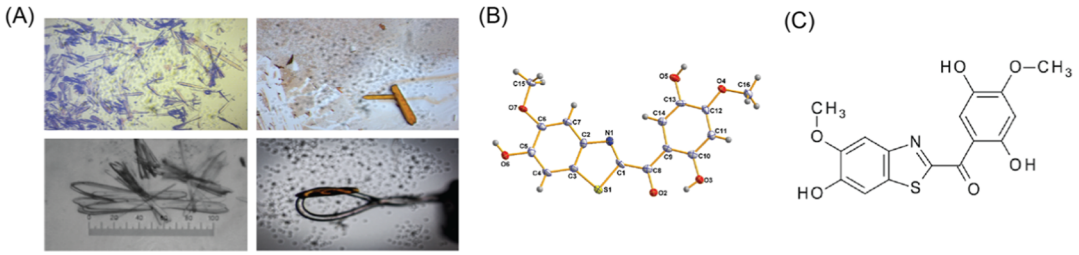

Figure 3. Isolated compound (F10V6W0) is a benzothiazole with a unique molecular structure, (A) microscopic view of the crystals of F10V6W0 (top left panel) against a measuring scale (bottom left panel), displaying their characteristic orange color (top right and bottom left panels). (B,C) Molecular structure of the isolated compound F10V6W0 from FWGE ((2,5-dihydroxy-4-methoxy-phenyl)-(6-hydroxy-5-methoxy-benzothiazol-2-yl) methanone).

ion at m/z 347.1 corresponded to the $[M + H]^+$ form of the inhibitor (348 Da). The major fragment ions (m/z 207.95, 181.97, and 166.95) were identified using a triple-quadrupole mass spectrometer (Figure S1E). High-resolution mass measurements were acquired on an Orbitrap Q-TOF instrument, providing mass accuracy to four decimal places (Figure 2E). Searches against the NIST compound database revealed no matches with a probability of >33%, suggesting that F10V6W0 may represent a novel small molecule.

The Isolated Compound (F10V6W0) Is a Benzothiazole with a Unique Molecular Structure

To determine the structure of the active component F10V6W0, isolated from FWGE, it was crystallized at room temperature, which generated orange crystals (Figure 3A). X-ray crystallography analysis revealed that the compound was a benzothiazole, (5-dihydroxy-4-methoxy-phenyl)-(6-hydroxy-5-methoxy-benzothiazol-2-yl)-methanone with a molecular weight of 347.34 (Figure 3B,C).

Although a ChemSpider search for the molecular formula of the compound ($C_{16}H_{13}NO_6S$) showed more than 2880 structures that shared the same molecular weight and 195 structures with the same molecular formula, none of them shared the same structure as F10V6W0, which makes it a unique and novel benzothiazole isolated from FWGE.

Chemical Synthesis, Structural Verification, and Quantification of CSH-4044

A core structural search using SciFinder revealed that although over 230 structural analogs of the lead inhibitor F10V6W0 had been reported, the specific compound was not commercially available. To enable further functional studies, the compound was chemically synthesized (Vichem Chemie Ltd., Budapest, Hungary; Figure 4A). The synthetic product was purified to >99% using a Waters preparative HPLC system. Its structure was confirmed by NMR spectroscopy and mass spectrometry, matching the spectral features of F10V6W0 isolated from FWGE (Figure S2A,B). Because the preparative HPLC system was equipped with a UV detector, the component at ∼347 Da was collected by monitoring UV absorbance at 418 nm, whereas the second component was collected at 334 nm (Figure S2C). The chemically synthesized version of F10V6W0 was named CSH-4044. During fermentation, the abundance of the active compound increased over time, with a higher signal detected at 8 h compared to 4 h of fermentation (Figure 4B), indicating that the fermentation step was crucial for the compound synthesis from wheat germ. To characterize CSH-4044, molecular weight and fragmentation data were obtained by using electron ionization mass spectrometry (ESI-MS) (Figure 4C).

Furthermore, CSH-4044 was assayed against a 138-kinase panel and displayed inhibition toward PIM and DYRK kinase families (Figure 4D, Table S2). To validate its synthetic route functionally, CSH-4044 was also tested with F10V6W0 from FWGE in kinase inhibition assays and was found to retain the same inhibitory activity as F10V6W0 against PIM3 and DYRK2 kinases (Figure 4E, Table 2). These results confirmed that the synthetic compound CSH-4044 replicates the in vitro kinase inhibitory activity of its natural counterpart, F10V6W0 from FWGE.

Crystal Structure of PIM1-CSH-4044 Complex

To investigate the structural basis of CSH-4044-mediated PIM1 inhibition, we determined the crystal structure of PIM1 in complex with CSH-4044. The PIM1-CSH-4044 co-crystals belong to space group $P6_5$ with one complex in the asymmetric unit. PIM1 has a typical bi-lobal serine/threonine kinase fold (Figure 5A, Table 3).

A clear difference in electron density due to CSH-4044 was observed, allowing us to place the inhibitor unambiguously in the ATP-binding pocket in a flat orientation between the two lobes of the kinase. The nucleotide binding pocket was lined by several hydrophobic residues (Leu44, Val52, Phe49, Ile104, Val126, Leu174, and Ile185) that surround the inhibitor. Moreover, the benzothiazole 5-methoxy group of CSH-4044 formed an H-bond with Lys67, whereas its 6-hydroxyl group H- bonded with Lys67 and the main-chain amide of Asp186. Additionally, the 6-hydroxyl group was stabilized by water-mediated interactions with Glu89 and the main-chain amide of Phe187 (Figure 5B). An Mg^{2+} ion is required for catalysis by PIM1 and is coordinated in an octahedral geometry via direct interactions with Ser189 and 5 water molecules, whereas catalytic Asp198 interacts directly with the water molecules coordinating the Mg^{2+} octahedron (Figure 5C). Similarly, the 2-hydroxyl group on the phenyl ring of CSH-4044 establishes water-mediated interactions with the Arg122 and Pro123 carbonyls, whereas its 4-methoxy group undergoes water-mediated interactions with the Asp131 and Asp128 amide groups (Figure 5D).

https://doi.org/10.1021/acs.jmedchem.5c03226
J. Med. Chem. 2026, 69, 7920−7932

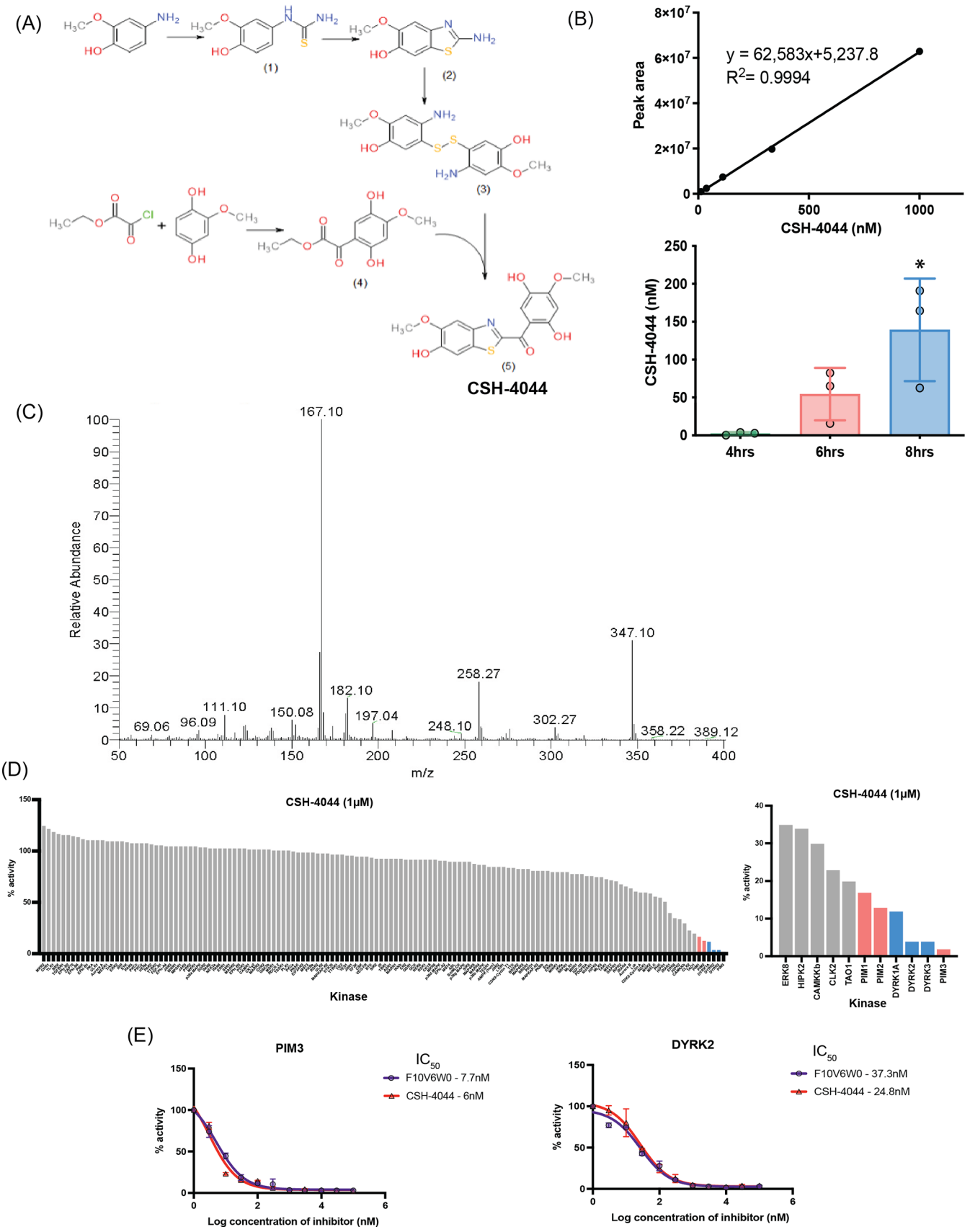

Figure 4. Chemical synthesis, structural verification, and quantification of CSH-4044, (A) flowchart outlining the steps involved in the chemical synthesis of CSH-4044. (B) Calibration curve (above) and HPLC-MS analysis (below) showing the abundance of CSH-4044 during the fermentation process at room temperature at three different time points (4, 6, and 8 h). *t*-test between 4 and 8 h (*$p < 0.05$; **$p < 0.005$; ***$p < 0.0005$; $p = 0.0245$). (C) Electrospray ionization mass spectrum (ESI-MS) of CSH-4044 showing the major fragment ions. (D) Waterfall plot of

https://doi.org/10.1021/acs.jmedchem.5c03226
J. Med. Chem. 2026, 69, 7920−7932

Figure 4. continued

the kinase selectivity panel (left) for the chemically synthesized compound CSH-4044 (1 μM). The PIM and DYRK kinases are labeled in red and blue, respectively. A selection of most-inhibited kinases by CSH-4044 is shown on the right. (E) IC_{50} of F10V6W0 from FWGE and chemically synthesized CSH-4044 against PIM3 and DYRK2 kinases (n = 2; biol. repeats).

Table 2. Comparison of Inhibitory Activity of the Isolated Compound with Synthetic CSH-4044 against PIM and DYRK Kinases (IC_{50} ± SD)[a]

kinase	isolated compound F10V6W0 IC_{50}	CSH-4044 IC_{50}
PIM3	7.7 nM (±1.8)	6 nM (±1.4)
DYRK2	37.3 nM (±2.8)	24.8 nM (±2.7)

[a]The assay was done with three (n = 3) biological repeats.

Notably, these hydrophobic interactions are very similar to the interaction with the adenine base in the PIM1-AMP-PNP structure (PDB 1XR1)[11] (Figure 5E), with the exception of P-loop Phe49, which repositions to occupy the β-phosphate position of AMP-PNP and closes the nucleotide binding pocket, as observed in the PIM1-Staurosporine structure (PDB 1YHS)[12] (Figure 5F). However, due to the polar nature of the CSH-4044, the direct H-bond interactions with Lys67 and Asp186 main-chain amide appear to be CSH-4044-specific.

CSH-4044 Inhibits PIMs and DYRKs in Two Cell-Based Models

To confirm that chemically synthesized CSH-4044 functioned as a kinase inhibitor in cells, multiple human cell lines were tested for endogenous expression of PIMs (PIM1, PIM2, and PIM3) and their downstream substrate, the pro-apoptotic protein BAD.[13−16] Among the eight lines tested, MiaPaCa-2, a human pancreatic cancer cell line, exhibited significant levels of all four proteins (Figure S3), making it suitable for functional validation. PIMs inhibit apoptosis by phosphorylating the pro-apoptotic protein BAD at Ser112 in pancreatic cancer.[8,13,14] Phosphorylation of BAD leads to its impaired binding to Bcl-XL and Bcl-2. The presence of unbound Bcl-XL eventually leads to the inhibition of apoptosis. Elevated PIM3 levels also increase BAD Ser112 phosphorylation, leading to apoptosis inhibition.[13,14,17] Treatment of MiaPaCa-2 cells with CSH-4044 markedly reduced phosphorylation of pBAD at Ser112 in MiaPaCa-2 (Figure 6A,B).

Since CSH-4044 is a dual PIM and DYRK kinase inhibitor, we also tested whether CSH-4044 can affect the phosphorylation of Tau at multiple residues. DYRK1A hyperphosphorylates Tau, leading to the formation of neurofibrillary tangles in Alzheimer's disease.[18,19] The ability of Tau to promote microtubule assembly was markedly reduced due to its phosphorylation by DYRK1A.[18−20] Using the cell-line SH-SY5Y, we observed that CSH-4044 could reduce Tau phosphorylation at three residues, Tau S212, S202/T205,

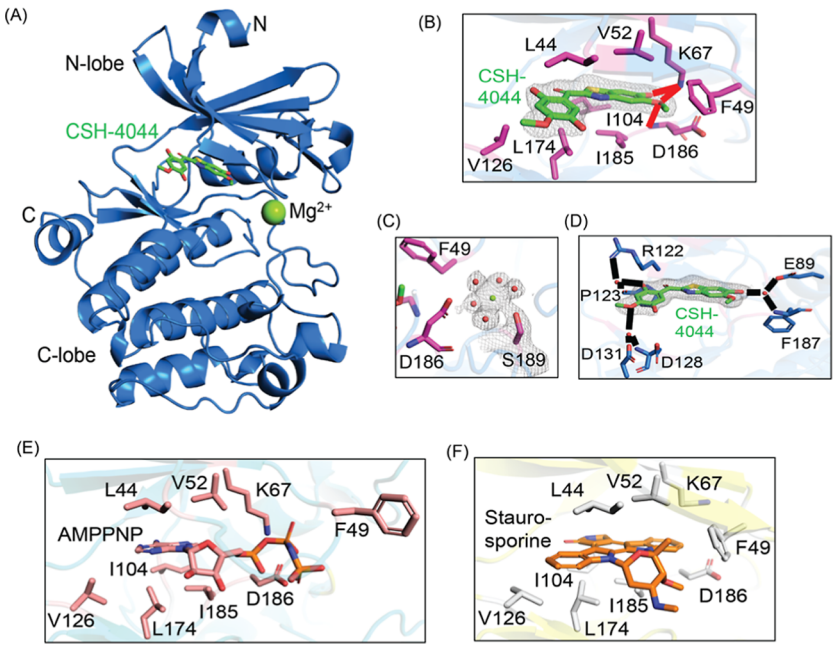

Figure 5. Crystal structure of human PIM1-CSH-4044 complex. (A) A cartoon representation of the PIM1 crystal structure in complex with the small molecule inhibitor CSH-4044, shown as sticks (green). (B) A close-up view of CSH-4044 in the PIM1 nucleotide binding site. The inhibitor is supported by several hydrophobic residues and direct H-bonds (red solid lines). The electron density shown for CSH-4044 is the observed 2Fo-Fc electron density shown as mesh at 1.0 σ level (carve radius of 1.6 Å). (C) The observed 2Fo-Fc electron density for the coordinated Mg^{2+} ion (green sphere) in the PIM1-CSH-4044 complex is shown as mesh at 1.0 s level (carve radius of 1.6 Å) together with coordinating water molecules (red spheres). Ser189 directly interacted with the Mg^{2+} ion, while Asp186 coordinates surrounding water molecules. (D) Close-up view of the water-mediated interaction network in CSH-4044 binding in PIM1. Zoom-in view of (E) AMP-PNP and (F) staurosporine inhibitor bound to PIM1 kinase. The hydrophobic residues stabilizing the AMP-PNP nucleotide and staurosporine are shown as sticks. Phe49 is repositioned in the staurosporine complex compared to the structure with AMP-PNP, to close the pocket. This repositioning is also observed in the complex with CSH-4044.

https://doi.org/10.1021/acs.jmedchem.5c03226
J. Med. Chem. 2026, 69, 7920−7932

Table 3. X-ray Data Collection and Structure Refinement Statistics for the Crystal Structure of the PIM1-CSH-4044 Complex[a]

	PIM-CSH-4044
PDB ID	9YKI
wavelength (Å)	1.0
space group	P65
a, *b*, *c* (Å)	97.93, 97.93, 80.40
α, *β*, *γ* (°)	90, 90, 120
resolution (Å)	41.82−1.94 (2.01−1.94)
no. of reflections	170,776
unique reflections	32,068
Rmerge (%)	4.7 (56.3)
<I/σ(I)>	20.6 (2.8)
$CC_{1/2}$	0.99 (0.81)
completeness (%)	99.77 (99.94)
multiplicity	5.3
refinement	
Rwork/Rfree	0.161/0.192
no. of residues	274
no. of nucleic acid	0
no. of hetero atoms	3
solvent atoms	177
R.M.S.D.	
bond lengths (Å)	0.018
bond angles (°)	1.55
ramachandran analysis	
most favored (%)	98.14
allowed (%)	1.49
outliers (%)	0.37
rotamer outlier (%)	0.4

[a](Values in parentheses represent the highest resolution shell).

and T231 (Figure 6C,D). This indicates that CSH-4044 could target PIMs and DYRKs in two cell-based models.

DISCUSSION

FWGE is a promising therapeutic agent for cancer and has been shown to exert antiproliferative and cytotoxic effects in several cell-based models.[21−23] In this study, we purified and identified a small-molecule inhibitor named CSH-4044 from a fraction of FWGE and characterized it as an inhibitor of the PIM and DYRK families of kinases using peptide-based kinase activity assays.

Considering the significance of PIMs in cancer, we determined the crystal structure of PIM1 in complex with CSH-4044. Several independent groups have reported the crystal structure of PIM1 and PIM2 kinases either in the presence or absence of inhibitors.[24−26] In agreement with previous crystal structures, we report that the PIM1 structure assumes a two-lobe kinase fold with a deep intervening cleft. The two lobes are connected by the hinge region, wherein several residues have been identified to bind ATP.[27] The ATP-binding pocket of PIMs adopts an open conformation, indicating that they are constitutively active.[25,26] PIMs are structurally unique due to the presence of a proline residue (Pro123) in the hinge region of their ATP-binding site.[28,29] The proline residue in PIMs, which is not usually observed in the case of other kinases, hinders the formation of a second bond between PIMs and ATP.[11,26] Our structural studies reveal that CSH-4044 is an ATP-competitive inhibitor of PIM1 kinase. This suggests that it may be possible to optimize and develop small-molecule inhibitors of PIMs by exploiting the interaction between the novel ATP-binding site and CSH-4044.

Most alterations in cancer are associated with signaling pathways that control cell growth and division, cell motility, cell death, and cell fate. Their dysregulation is often responsible for mediating distortions of wider signaling networks fueling cancer progression.[30] Kinases often form part of the commonly altered signaling pathways in cancer.[31] The PIM family of kinases has been implicated in tumorigenesis due to their constitutive activity and ability to regulate multiple survival and growth pathways.[24,32−40] PIM3 contributes to pancreatic ductal adenocarcinoma progression by phosphorylating the pro-apoptotic protein BAD at Ser112, thereby blocking its apoptotic activity.[17,41,42] We show that CSH-4044 inhibits PIM activity in vitro and reduces the level of phosphorylation of BAD in MiaPaCa-2, supporting a direct intracellular effect.

In addition to PIMs, out of all of the kinases tested, the chemically synthesized CSH-4044 demonstrated inhibition of the DYRK family of kinases. DYRK1A phosphorylates a range of substrates,[9,43−46] including Tau, where it promotes pathological hyperphosphorylation linked to Alzheimer's disease.[18−20] In SH-SY5Y cells, a neuroblastoma cell line used widely as a model for studying neuronal features, treatment with CSH-4044 decreased phosphorylation of Tau at multiple residues, consistent with the inhibition of DYRK activity. These results extend the biological activity of CSH-4044 beyond oncology and highlight its potential utility in modulating kinase pathways associated with neurodegeneration.

Taken together, this study establishes CSH-4044 as a unique benzothiazole scaffold with a dual inhibitory activity against PIM and DYRK kinases. Our results also highlight a source of structurally novel bioactive compounds and underscore the potential of nutraceutical-derived metabolites to yield selective small-molecule kinase inhibitors.

CONCLUSION

Despite the importance of PIM as a target in cancer and the fact that ATP-competitive, small-molecule PIM inhibitors have been tested in clinical trials against different cancers, including prostate, myeloma, lymphoma, and acute myelogenous leukemia, to date, there are no FDA-approved PIM inhibitors.[28,29,47] Consequently, the development of PIM inhibitors is an unmet need. Our study identifies CSH-4044 as a novel, ATP-competitive inhibitor of PIMs and DYRKs, with therapeutic potential in pancreatic cancer and neurodegenerative diseases such as Alzheimer's. These findings underscore the value of nutraceutical-derived scaffolds as a source of structurally unique and biologically potent drug candidates.

EXPERIMENTAL SECTION

FWGE Component Separation and Extraction

Commercially available freeze-dried FWGE (10 g) obtained from American Biosciences, Inc., was resuspended in 30 mL of analytical grade methanol (Sigma-Aldrich) and sonicated for 5 min. The insoluble solids were separated with a glass Buchner filtering funnel combined with quantitative grade filter paper. The pellet was resuspended (Fraction A1) in methanol and filtered again. The filtrates were combined, and a Büchi Rotavapor R-100 benchtop evaporator system was used to remove the solvent, leaving the soluble

https://doi.org/10.1021/acs.jmedchem.5c03226
J. Med. Chem. 2026, 69, 7920−7932

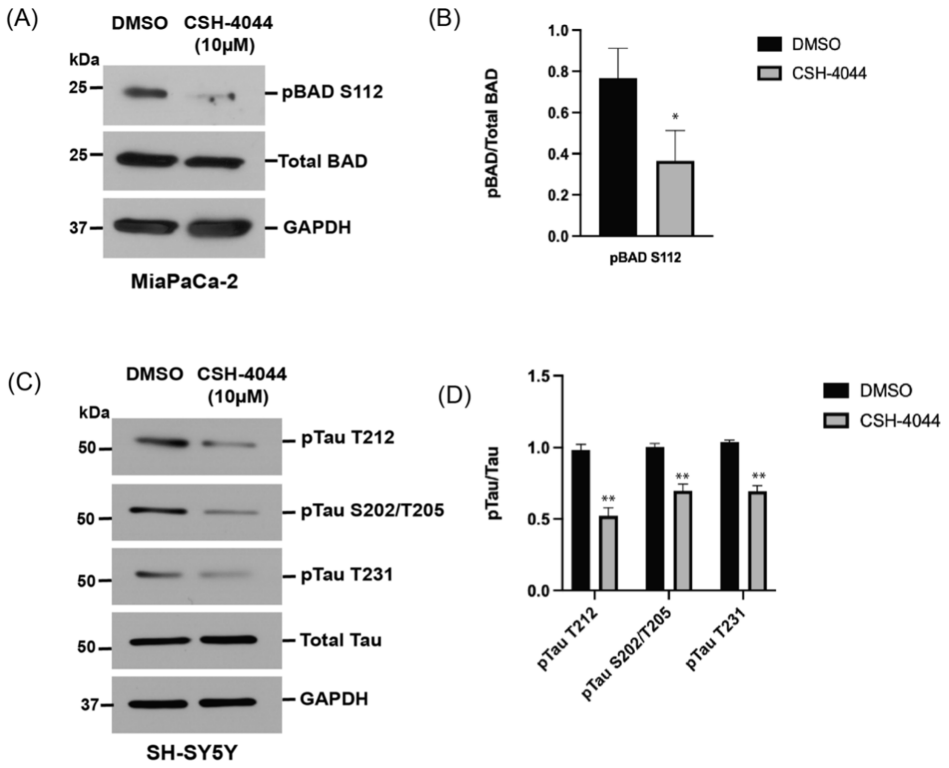

Figure 6. CSH-4044 inhibits PIMs and DYRKs in two cell-based models. (A,B) CSH-4044 (10 μM) reduces phosphorylation of BAD Ser112 in MiaPaCa-2 compared to the DMSO control (n = 3 biological repeats). Bars represent mean ± SEM. (C,D) CSH-4044 reduces Tau phosphorylation at Ser212, Ser202/205, and Thr231 in SH-SY5Y cells (n = 3 biological repeats). Bars represent mean ± SEM.

part of FWGE behind (Fraction A2). Fraction A2 was dissolved in 80 mL of distilled water and was passed through a SPE column (Hydrophile Lipophile Balance, HLB, Waters). The column was washed with 50 mL of water, and the isolated components from the column were eluted with 50% methanol. The excess methanol was removed with the Büchi Rotavapor R-100 benchtop evaporator system. The samples were flash frozen in liquid nitrogen and lyophilized using a Labconco FreeZone 6 Plus freeze-dryer (Fraction A250). Next, fraction A250 was resuspended in 200 mL of distilled water, and its pH was adjusted to 2. Analytical grade ethyl acetate (Sigma-Aldrich) was used to perform liquid–liquid extraction. The upper phases were collected, and the residual moisture was removed using magnesium sulfate (Sigma-Aldrich) after combining the extracts. Finally, the solvent was removed from the ethyl acetate soluble extract (Fraction A252E) using a Büchi Rotavapor R-100 benchtop evaporator system.

Preparative Scale High-Performance Liquid Chromatography—Reverse Phase

Waters AutoPurification system was used for the preparative HPLC, which consisted of the 2545 binary gradient module, 2767 injector/collector sample manager, system fluidics organizer, and 2998 photodiode array detector. The samples were dissolved in 80% DMSO (Sigma-Aldrich). They were injected onto a Phenomenex Luna phenyl-hexyl 100A (5 mL) (250 × 50 mm, 10 μm) or Phenomenex Luna C18(2) 100A (250 × 21.5 mm, 5 μm) columns to separate components. The flow rate was 42.48 mL/min, and the eluents were: "eluent A" was analytical grade Water (Sigma-Aldrich) with 0.05% formic acid (Sigma-Aldrich), and "eluent B" was analytical grade acetonitrile (Sigma-Aldrich) with 0.05% formic acid. The gradient was the following: 0 min 95% A, 1 min 75% A, 86.76 min 70% A, 91.67 min 5% A, 96.67 min 5% A, and 100 min 95% A. The fractions were collected continuously between 5 and 25 min. When the PDA detector triggered a fraction at a specific absorbance, the components were collected. The system was controlled by the Waters MassLynx 4.1 software with the FractionLynx add-on.

Liquid–Liquid Extraction of the Lipophilic Part

50g of Fraction A250 (50 g) was resuspended in water. The pH was adjusted to 2 with hydrochloric acid (Sigma-Aldrich) and was extracted twice with ethyl acetate (Sigma-Aldrich). The extract was dried with magnesium sulfate (Sigma-Aldrich) and filtered with a Buchi glass filter utilizing a quantitative grade filter paper (Millipore). The solvent was removed under vacuum at 50 ^{o}C using a Buchi Rotavapor R-100 benchtop evaporator system.

Flash Chromatography

A Teledyne Combiflash Companion Chromatography System with RediSep Rf chromatography column prepacked with 80 g of normal phase silica was used to separate the components of the concentrated fractions. Eluent A was analytical grade hexane (Sigma-Aldrich), and eluent B was analytical grade ethyl acetate. The flow rate was set to 60 mL/min, the gradient was 2 min 100% A, 27 min 100% B for 4 min, and then 100% A for 3 min. The sample was dissolved in methanol at a very high concentration. The fractions were collected continuously from the beginning of the run. Selected fractions were dried with a Genevac EZ-2 Plus Personal in a 20 mL sample vial.

Preparative Scale HPLC Purification

The Waters AutoPurification system, consisting of the 2545 binary gradient module, 2767 injector/collector sample manager, system fluidics organizer, and 2998 photodiode array detector, was used to isolate fractions of A252. Samples were dissolved in dimethyl sulfoxide (Sigma-Aldrich) at very high concentration and injected in up to 5 mL volume on to a Phenomenex Luna Phenyl-Hexyl 100A (250 × 50 mm, 10u) or Phenomenex Luna C18(2) 100A (250 × 21.5 mm, 5 μm) columns to separate components. The flow rate was 42.48 mL/min. The eluents were the following: "eluent A" was analytical grade water (Sigma-Aldrich) with 0.05% formic acid (Sigma-Aldrich), and "eluent B" was analytical grade acetonitrile (Sigma-Aldrich) with 0.05% formic acid. The gradient was the following: 0 min 95% A, 1 min 75% A, 86.76 min 70% A, 91.67 min 5% A, 96.67 min 5% A, and 100 min 95% A. The fractions were collected either continuously between 5 and 25 min of the run, or the collection was triggered by

https://doi.org/10.1021/acs.jmedchem.5c03226
J. Med. Chem. 2026, 69, 7920−7932

the PDA detector at a specified absorbance in case a specific component was collected. The system was controlled by the Waters MassLynx 4.1 software with the FractionLynx add-on. All compounds are >95% pure by HPLC.

Mass Spectrometry (LC–MS/MS)

A Thermo Scientific TSQ Vantage Triple Quadrupole mass spectrometer was used to quantify the isolated inhibitor in the fermentation broth. The sample was eluted from a Thermo Accela HPLC system equipped with a Thermo Scientific Aquasil C18 Column (100 mm × 2.1 mm, 3 μm). The flow rate was 100 μL/min, and the eluents were analytical grade water (Sigma-Aldrich) with 0.05% formic acid (Sigma-Aldrich) as eluent A, and analytical grade acetonitrile (Sigma-Aldrich) with 0.05% formic acid as eluent B. The synthetic compound with verified purity was used for tuning and calibration. The main parameters of the detector were capillary temperature 320 °C, vaporizer temperature 300 °C, sheath gas pressure 30 psi, auxiliary gas flow 25, and spray voltage 3000 V. The parent ion of the inhibitor was 347.966 Da, and the most abundant daughter ions were 166.975, 181.971, 207.949, and 225.969 Da.

Peptide-Based Kinase Assay

The radiometric peptide-based kinase assay was performed to validate the results and determine the IC_{50} of the inhibitors using the protocol described in ref 48. The recombinant His-tagged (N-terminus) DYRK1A (127-485aa) and PIM1 kinases (313aa) were purified from bacterial BL21 cells using Ni-NTA beads and assayed against the peptide sequences KKISGRLSPIMTEQ and RSRHSSYPAGT (gift from the University of Dundee) for DYRK1A and PIM1, respectively, at a final concentration of 10 mM in the assay buffer containing 25 mM HEPES, pH 6.8, 5 mM $MgCl_2$, 0.5 mM DTT, and 1 mg/mL BSA. The [γ-^{32}P] ATP for the assay was purchased from PerkinElmer (#BLU502A250UC). The specific activity of [γ-^{32}P] ATP was determined by dissolving and spiking nonradioactive "cold" ATP (Sigma) in assay buffer using [γ-^{32}P] ATP to produce radioactivity of 1×10^5 to 1×10^6 cpm per nmol. The kinase assay done either with or without inhibitors, was performed at 30 °C with a 10 min incubation period. The reaction mixture (15 μL) was then spotted onto 2 × 2 P81 phospho-cellulose papers (Whatman) that bind the peptide substrate. The excess ATP was then washed from the P81 papers using 75 mM phosphoric acid using a mesh basket, three times, followed by a final wash using acetone. The P81 papers were dried and measured for radioactivity with a scintillation counter (GMI). The data were then plotted using GraphPad Prism.

Chemical Synthesis of CSH-4044 (2,5-Dihydroxy-4-methoxy-phenyl)-(6-hydroxy-5-methoxy-benzothiazol-2-yl)-methanone

All compounds are >95% pure by HPLC.

4-(Hydroxy-3-methoxy-phenyl)-Thiourea (1). A mixture of 1.39 g (10.0 mmol) 4-amino-2-methoxyphenol, 2.18 mL of water, and 0.78 mL of hydrochloric acid (37%) was stirred at 80 °C in a closed vessel for 1 h, then 0.76 g (10 mmol) of ammonium thiocyanate was added, and the stirring was continued at 120 °C for 1 day. The reaction mixture was diluted with water, and the precipitate was filtered out, washed with water and a small amount of acetone, and then dried in air. Thus, 1.48 g of the title compound was obtained (yield 75%). LC–MS Anal. Calculated for $C_8H_{10}N_2O_2S$, 198.25; found m/z: 197 $[M - H]^-$, 199 $[M + H]^+$, tR = 0.46 and 1.21 min; peak area 99%.

2-Amino-6-hydroxy-5-methoxy-Benzothiazole (2). To the solution of 1.43g (7.21 mmol) (4-hydroxy-3-methoxy-phenyl)-thiourea (1) in 42 mL of acetic acid, 2.84g (7.28 mmol) benzyltrimethylammonium tribromide was added in portions, and then the mixture was stirred at room temperature for 1 h. The precipitated hydrogenbromide salt was filtered out and washed with acetic acid and di-isopropyl ether. This solid was dissolved in a saturated aqueous solution of sodium bicarbonate and then extracted three times with ethyl acetate. The organic layers were combined, washed with brine, dried over anhydrous sodium sulfate, and filtered, and the solvent was evaporated. The residue solidified under di-isopropyl ether. Thus, 1.05 g of 2-amino-5-methoxy-benzothiazol-6-ol (2) was obtained (yield: 74%). Melting point: 183–185 °C. 1H NMR (300 MHz, DMSO-d_6): δ 8.59 (s, 1H), 7.05 (s, 2H), 7.01 (s, 1H), 6.93 (s, 1H), 3.76 (s, 3H). LCMS Anal. Calculated for $C_8H_8N_2O_2S$, 196.23; found m/z: 197 $[M + H]^+$, tR = 0.46 and 1.42 min; peak area 97%.

Bis(4-Hydroxi-5-methoxyanilin-2-yl)disulfide (3). A mixture of 3000 mg of potassium hydroxide, 9 mL of water, and 1.00g (5.09 mmol) 2-amino-6-hydroxy-5-methoxy-benzothiazole was refluxed for 6 h. The cooled solution was neutralized with acetic acid, and then, sodium hydrogen carbonate solution was added. The solution was extracted three times with ethyl acetate. The organic phases were combined, washed with brine, dried over anhydrous sodium sulfate, and filtered, and the solvent was evaporated in a vacuum. The residue solidified under di-isopropyl ether. Thus, 632 mg of the title compound was obtained (yield 81%). 1H NMR (300 MHz, DMSO-d_6): δ 8.15 (s, 2H), 6.55 (s, 2H), 6.35 (s, 2H), 4.83 (s, 4H), 3.70 (s, 6H). LC–MS Anal. Calculated for $C_{14}H_{16}N_2O_4S_2$, 340.42; found m/z: 339 $[M + H]^-$, 341 $[M + H]^+$, tR = 0.46, and 2.07 min; peak area 96%.

(2,5-Dihydroxy-4-methoxy-phenyl)-oxo-Acetic Acid Ethyl Ester (4). 1.4 g (10 mmol) portion of 2,5-dihydroxyanisole and 1.38g (10.1 mmol) of ethyl oxalyl chloride were dissolved in 100 mL of anhydrous dichloromethane and stirred at −15 °C. Then 12 mL of 1 M solution of titanium tetrachloride in dichloromethane was added dropwise to the reaction mixture at −15 °C for 30 min, and the stirring was continued for a further 2 h at −15 °C. 150 mL of 1 M hydrochloric acid was added to the reaction mixture, and then the mixture was stirred at room temperature for 1 h. The two layers were separated, the aqueous layer was extracted two times with dichloromethane, the organic layers were combined and washed with 100 mL of water, then with 50 mL of saturated sodium hydrogen carbonate solution and 100 mL of water, and the organic layer was separated and dried over sodium sulfate, filtered, and evaporated in vacuum. The residue solidified under hexane. Thus, 1.072g of the title compound was obtained (yield 39%). Melting point: 131–132 °C. 1H NMR (300 MHz, DMSO-d_6): δ 10.60 (s, 1H), 9.00 (s, 1H), 7.04 (s, 1H), 6.46 (s, 1H), 4.31–4.24 (q, J = 7.2 Hz, 2H), 1.30–1.25 (t, J = 7.2 Hz, 3H). LCMS Anal. Calculated for $C_{11}H_{12}O_6$, 240.21; found m/z: 239 $[M + H]^-$, 241 $[M + H]^+$, tR = 2.99 min; peak area 99%.

(2,5-Dihydroxy-4-methoxy-phenyl)-(6-hydroxy-5-methoxy-benzothiazol-2-yl)-Methanone (5). 408 mg (1.2 mmol) portion of disulfide (3) and 312 mg (1.2 mmol) of triphenylphosphine were stirred in aqueous ethyl alcohol (2.4 mL of water and 2.4 mL of ethyl alcohol) under an argon atmosphere for 1 h at room temperature. Then 652 mg (2.4 mmol) of ester (4) was added, argon was passed through the mixture for 10 min, the vessel was closed, and it was put into a microwave oven for 2.5 h at 130 °C. The precipitate was filtered at room temperature, washed with ethyl alcohol and di-isopropyl ether, and then dried in air. The crude product was purified by preparative HPLC. Thus, 350 mg of the title compound was obtained (yield 42%). ^{1}H NMR (300 MHz, DMSO-d_6): δ 12.46 (s, 1H), 10.12 (b, 1H), 8.96 (s, 1H), 8.66 (s, 1H), 7.72 (s, 1H), 7.51 (s, 1H), 6.60 (s, 1H), 3.93 (s, 3H), 3.90 (s, 3H). LCMS Anal. Calculated for $C_{16}H_{13}NO_6S$, 347.35; found m/z: 346 $[M + H]$, 348 $[M + H]^+$, tR = 3.54 min; peak area 99%.

Protein Expression, Purification, and Crystallization

Human PIM1 (PIM1) (1-313aa) was cloned into the pET28 expression vector with N-terminal 6XHis and SUMO tags, followed by a TEV protease cleavage site. The protein was expressed in *E. coli* (BL21 DE3) for 16 h at 20 °C. Cells were resuspended and lysed by sonication in 50 mM Tris, pH = 8.0, 100 mM NaCl, 40 mM imidazole, and 2 mM $CaCl_2$. Protein was initially purified using Ni-NTA agarose resin (Qiagene), followed by on-column TEV protease cleavage. Further purification was carried out using a Q-HP column (Cytiva), followed by final purification using a HiLoad Superdex 75 column (Cytiva). Protein was stored in the following buffer: 20 mM Tris, pH = 8.0, 100 mM NaCl, 2 mM $MgCl_2$, 2 mM $CaCl_2$, 0.5 mM TCEP, and 5 mM DTT at 5 mg/mL. The protein was crystallized

https://doi.org/10.1021/acs.jmedchem.5c03226
J. Med. Chem. 2026, 69, 7920–7932

using the vapor diffusion sitting drop method by mixing 500 nL of the protein with 500 nL of 0.2 M NaCl, 0.2 M $CaCl_2$, 0.1 M trisodium-citrate, pH = 5.5, and 1 M diammonium hydrogen phosphate precipitant solution at 18 °C. Crystals were then soaked in 0.2 M NaCl, 0.2 M $CaCl_2$, 0.1 M trisodium-citrate, pH = 5.5, and 1 M diammonium hydrogen phosphate, Supporting Information, with 10 mM CSH-4044 overnight. Crystals were cryoprotected by transferring them briefly to a solution containing 0.2 M NaCl, 0.2 M $CaCl_2$, 0.1 M trisodium-citrate, pH = 5.5, 1 M diammonium hydrogen phosphate, and 30% glycerol before flash freezing in liquid nitrogen.

Data Collection and Structure Determination

Data were collected to a resolution of 1.95 Å at beamline 8.2.1 at the Berkeley center for structural biology at the advanced light source. Diffraction data were indexed, integrated, and scaled using autoPROC.[49] The structure was solved by molecular replacement in PHASER[50] using the Apo PIM1 structure as a search model (PDB: 1XQZ).[25] The molecular replacement solution was rigid-body refined in PHENIX followed by simulated annealing refinement prior to manual correction in COOT.[51] The final refinement of the model was done using PHENIX[52] and validated by Molprobity.[53] X-ray data collection and refinement statistics for the PIM1-CSH-4044 structure are summarized in Table 3. The atomic coordinates and structure factors for PIM1-CSH-4044 structure have been deposited in the Protein Data Bank under accession code 9YKI.

Structure Determination of CSH-4044 Using X-ray Crystallography

The structure of the isolated compound CSH-4044 was determined at New York University, New York (NYU) by Dr. Chunhuao Tony Hu. A red needle-like crystal with the size of 0.01 × 0.05 × 0.28 mm^3 was selected for geometry and intensity data collection with a Bruker SMART APEXII CCD area detector on a D8 goniometer at 100 K. The temperature during the data collection was controlled with an Oxford Cryosystems Series 700 plus instrument. Preliminary lattice parameters and orientation matrices were obtained from three sets of frames. Data were collected using graphite-monochromated and 0.5 mm MonoCap-collimated Mo-Ka radiation (λ = 0.71073 Å) with the ω scan method. Data was processed with the INTEGRATE program of the APEX2 software for reduction and cell refinement. Multiscan absorption corrections were applied by using the SCALE program for the area detector. The structure was solved by a direct method and refined on F2 (SHELXTL). Non-hydrogen atoms were refined with anisotropic displacement parameters, and hydrogen atoms on carbons and oxygens were placed in idealized positions (C−H = 0.95−0.98 Å and O−H = 0.84 Å) and included as riding with Uiso(H) = 1.2 or 1.5 Ueq(non-H).

Cell-Based Assays

The cell-lines MiaPaca-2 and SH-SY5Y were obtained from ATCC and were maintained in Dulbecco's Modified Eagle's Medium (DMEM) and DMEM/F12 with 10% FBS, respectively. After treatment with CSH-4044 or DMSO, whole cell lysates were harvested and resuspended in RIPA buffer [25 mM Tris, pH 7.4, 150 mM NaCl, 1% Triton X 100, 0.5% sodium deoxycholate, 0.1% sodium dodecyl sulfate, and protease inhibitor cocktail (Sigma, Cat. no. 4693159001), and phosphatase inhibitor cocktail (Sigma, Cat. no. 4906845001)]. Quantification of protein concentration was done using the Pierce BCA Protein Assay kit (Thermo Fisher, Cat. no. 23225). Equal amounts of the lysate were denatured and loaded onto a 10% SDS-PAGE gel. Antibody blocking was done with 5% milk in TBST (19 mM Tris base, NaCl 137 mM, KCl 2.7 mM, and 0.1% Tween-20) for 1 h at room temperature. Blots were incubated with the primary antibody pBAD Ser112 (Cell Signaling Technologies, Cat. no. 9291), pTau T212, pTau S202/T205, pTau T231, and Total Tau (Thermo Fisher Scientific, Cat. nos. 44-740G, MN1020, MA5-12808, MN1040) overnight at 4 °C. Membranes were washed three times at room temperature (10 min each) before they were incubated with secondary antibodies for 1 h at room temperature. HRP goat antimouse (Bio-Rad; Cat. no. 1706516) at 1:50,000 was used for tubulin blots, while HRP goat antirabbit (Abcam, Cat. no. ab6721) at 1:30,000 was used for all other primary antibodies. Membranes were washed 3 times again (15 min each) and developed using SuperSignal West Dura Extended Duration Substrate (Thermo Fisher, Cat. no. 34075) and BioExcell autoradiographic film (Worldwide Medical, Cat. no. 41101001).

■ ASSOCIATED CONTENT

Data Availability Statement

The atomic coordinates and structure factors for the PIM1-CSH-4044 structure have been deposited in the Protein Data Bank under accession code 9YKI. Authors will release the atomic coordinates and experimental data upon article publication.

Supporting Information

The Supporting Information is available free of charge at https://pubs.acs.org/doi/10.1021/acs.jmedchem.5c03226.

Enrichment of Fraction A250 from FWGE; H NMR and UV chromatograms of F10V6W0 and CSH-4044 inhibitor molecules; and immunoblot screening of PIM1, PIM2, PIM3, and BAD in different cell lines (PDF)

Molecular formula string (CSV)

Kinase selectivity panel showing percentage activity of the isolated compound F10V6W0 (1 μM) against 138 kinases; kinase selectivity panel showing percentage activity of the synthesized compound CSH-4044 (1 μM) against 138 kinases (CSV)

■ AUTHOR INFORMATION

Corresponding Author

Nicholas K. Tonks − *Cold Spring Harbor Laboratory, New York, New York 11724, United States*; Email: tonks@cshl.edu

Authors

Gyula Bencze − *Cold Spring Harbor Laboratory, New York, New York 11724, United States*

Prabhadevi Venkataramani − *Cold Spring Harbor Laboratory, New York, New York 11724, United States*; orcid.org/0000-0001-9106-0102

Elad Elkayam − *Cold Spring Harbor Laboratory, New York, New York 11724, United States; Howard Hughes Medical Institute, New York, New York 11724, United States*

Keith D. Rivera − *Cold Spring Harbor Laboratory, New York, New York 11724, United States*

Ankur Garg − *Cold Spring Harbor Laboratory, New York, New York 11724, United States; Howard Hughes Medical Institute, New York, New York 11724, United States*

Istvan Szabadakai − *Vichem Chemie Ltd, Budapest 1045, Hungary*

Laszlo Orfi − *Vichem Chemie Ltd, Budapest 1045, Hungary; Pharmacy Faculty of Semmelweis University, Budapest 1085, Hungary*

Leemor Joshua-Tor − *Cold Spring Harbor Laboratory, New York, New York 11724, United States; Howard Hughes Medical Institute, New York, New York 11724, United States*

Darryl J. Pappin − *Cold Spring Harbor Laboratory, New York, New York 11724, United States*; orcid.org/0000-0002-8981-8401

Complete contact information is available at: https://pubs.acs.org/10.1021/acs.jmedchem.5c03226

https://doi.org/10.1021/acs.jmedchem.5c03226
J. Med. Chem. 2026, 69, 7920−7932

Author Contributions

[⊥]G.B. and P.V. contributed equally to this study.

Funding

N.K.T. is the Caryl Boies Professor of Cancer Research at Cold Spring Harbor Laboratory. This work was supported by the Cold Spring Harbor Laboratory and Northwell Health Affiliation. Research in the Tonks lab is also supported by NIH grant R01CA53840, the CSHL Cancer Centre Support Grant CA45508, and the Hansen Foundation.

Notes

The authors declare no competing financial interest.

■ ACKNOWLEDGMENTS

We thank Dr. Chunhua Hu and the NYU Molecular Design Institute for assistance with data collection and structure determination of CSH-4044. We thank Dr. James D. Watson for his encouragement and his generous personal donation that enabled the purchase of the preparative-scale HPLC system used for fractionating the extract and isolating the inhibitor compound. His support was instrumental to the success of this project.

■ ABBREVIATIONS USED

BAD; pro-apoptotic protein Bcl-2-associated death promoter; DMEM; Dulbecco's Modified Eagle's Medium; DMBQ; 2,6-dimethoxyhydroquinone; DMSO; dimethyl sulfoxide; DYRK; dual-specificity, tyrosine phosphorylation-regulated kinase; F12; Ham's F-12 nutrient mixture; FBS; fetal bovine serum; FWGE; fermented wheat germ extract; MS; mass spectrometry; PIM; proviral integration site for Moloney murine leukemia virus kinase; Q-TOF; Quadrupole time-of-flight

■ REFERENCES

(1) Zhurakivska, K.; Troiano, G.; Caponio, V. C. A.; Dioguardi, M.; Arena, C.; Lo Muzio, L. The Effects of Adjuvant Fermented Wheat Germ Extract on Cancer Cell Lines: A Systematic Review. *Nutrients* **2018**, *10* (10), 1546.

(2) Imir, N. G.; Aydemir, E.; Şimşek, E. Mechanism of the Anti-Angiogenic Effect of Avemar on Tumor Cells. *Oncol. Lett.* **2017**, *15* (2), 2673−2678.

(3) Mueller, T.; Jordan, K.; Voigt, W. Promising Cytotoxic Activity Profile of Fermented Wheat Germ Extract (Avemar®) in Human Cancer Cell Lines. *J. Exp. Clin. Cancer Res.* **2011**, *30*, 42.

(4) Judson, P. L.; Al Sawah, E.; Marchion, D. C.; Xiong, Y.; Bicaku, E.; Zgheib, N. B.; Chon, H. S.; Stickles, X. B.; Hakam, A.; Wenham, R. M.; Apte, S. M.; Gonzalez-Bosquet, J.; Chen, D.-T.; Lancaster, J. M. Characterizing the Efficacy of Fermented Wheat Germ Extract against Ovarian Cancer and Defining the Genomic Basis of Its Activity. *Int. J. Gynecol. Cancer* **2012**, *22* (6), 960−967.

(5) Yang, M.-D.; Chang, W.-S.; Tsai, C.-W.; Wang, M.-F.; Chan, Y.-C.; Chan, K.-C.; Lu, M.-C.; Kao, A.-W.; Hsu, C.-M.; Bau, D.-T. Inhibitory Effects of AVEMAR on Proliferation and Metastasis of Oral Cancer Cells. *Nutr. Cancer* **2016**, *68* (3), 473−480.

(6) Telekes, A.; Hegedus, M.; Chae, C.-H.; Vékey, K. Avemar (Wheat Germ Extract) in Cancer Prevention and Treatment. *Nutr. Cancer* **2009**, *61* (6), 891−899.

(7) Hidvégi, M.; Ráso, E.; Tömösközi-Farkas, R.; Paku, S.; Lapis, K.; Szende, B. Effect of Avemar and Avemar + Vitamin C on Tumor Growth and Metastasis in Experimental Animals. *Anticancer Res.* **1998**, *18* (4A), 2353−2358.

(8) Nawijn, M. C.; Alendar, A.; Berns, A. For Better or for Worse: The Role of Pim Oncogenes in Tumorigenesis. *Nat. Rev. Cancer* **2011**, *11* (1), 23−34.

(9) Fernández-Martínez, P.; Zahonero, C.; Sánchez-Gómez, P. DYRK1A: The Double-Edged Kinase as a Protagonist in Cell Growth and Tumorigenesis. *Mol. Cell. Oncol.* **2015**, *2* (1), No. e970048.

(10) Bencze, G.; Bencze, S.; Rivera, K. D.; Watson, J. D.; Hidvegi, M.; Orfi, L.; Tonks, N. K.; Pappin, D. J. Mito-Oncology Agent: Fermented Extract Suppresses the Warburg Effect, Restores Oxidative Mitochondrial Activity, and Inhibits in Vivo Tumor Growth. *Sci. Rep.* **2020**, *10* (1), 14174.

(11) Kumar, A.; Mandiyan, V.; Suzuki, Y.; Zhang, C.; Rice, J.; Tsai, J.; Artis, D. R.; Ibrahim, P.; Bremer, R. Crystal Structures of Proto-Oncogene Kinase Pim1: A Target of Aberrant Somatic Hypermutations in Diffuse Large Cell Lymphoma. *J. Mol. Biol.* **2005**, *348* (1), 183−193.

(12) Jacobs, M. D.; Black, J.; Futer, O.; Swenson, L.; Hare, B.; Fleming, M.; Saxena, K. Pim-1 Ligand-Bound Structures Reveal the Mechanism of Serine/Threonine Kinase Inhibition by LY294002. *J. Biol. Chem.* **2005**, *280* (14), 13728−13734.

(13) Aho, T. L. T.; Sandholm, J.; Peltola, K. J.; Mankonen, H. P.; Lilly, M.; Koskinen, P. J. Pim-1 Kinase Promotes Inactivation of the pro-Apoptotic Bad Protein by Phosphorylating It on the Ser [112] Gatekeeper Site. *FEBS Lett.* **2004**, *571* (1−3), 43−49.

(14) Yan, B.; Zemskova, M.; Holder, S.; Chin, V.; Kraft, A.; Koskinen, P. J.; Lilly, M. The PIM-2 Kinase Phosphorylates BAD on Serine 112 and Reverses BAD-Induced Cell Death. *J. Biol. Chem.* **2003**, *278* (46), 45358−45367.

(15) Li, Y.-Y.; Popivanova, B. K.; Nagai, Y.; Ishikura, H.; Fujii, C.; Mukaida, N. Pim-3, a Proto-Oncogene with Serine/Threonine Kinase Activity, Is Aberrantly Expressed in Human Pancreatic Cancer and Phosphorylates Bad to Block Bad-Mediated Apoptosis in Human Pancreatic Cancer Cell Lines. *Cancer Res.* **2006**, *66* (13), 6741−6747.

(16) Popivanova, B. K.; Li, Y.-Y.; Zheng, H.; Omura, K.; Fujii, C.; Tsuneyama, K.; Mukaida, N. Proto-Oncogene, Pim-3 with Serine/Threonine Kinase Activity, Is Aberrantly Expressed in Human Colon Cancer Cells and Can Prevent Bad-Mediated Apoptosis. *Cancer Sci.* **2007**, *98* (3), 321−328.

(17) Liu, B.; Wang, Z.; Li, H.-Y.; Zhang, B.; Ping, B.; Li, Y.-Y. Pim-3 Promotes Human Pancreatic Cancer Growth by Regulating Tumor Vasculogenesis. *Oncol. Rep.* **2014**, *31* (6), 2625−2634.

(18) Ryoo, S.-R.; Jeong, H. K.; Radnaabazar, C.; Yoo, J.-J.; Cho, H.-J.; Lee, H.-W.; Kim, I.-S.; Cheon, Y.-H.; Ahn, Y. S.; Chung, S.-H.; Song, W.-J. DYRK1A-Mediated Hyperphosphorylation of Tau. A Functional Link between Down Syndrome and Alzheimer Disease. *J. Biol. Chem.* **2007**, *282* (48), 34850−34857.

(19) Yin, X.; Jin, N.; Shi, J.; Zhang, Y.; Wu, Y.; Gong, C.-X.; Iqbal, K.; Liu, F. Dyrk1A Overexpression Leads to Increase of 3R-Tau Expression and Cognitive Deficits in Ts65Dn Down Syndrome Mice. *Sci. Rep.* **2017**, *7* (1), 619.

(20) Chaves, J. C. S.; Machado, F. T.; Almeida, M. F.; Bacovsky, T. B.; Ferrari, M. F. R. microRNAs Expression Correlates with Levels of APP, DYRK1A, Hyperphosphorylated Tau and BDNF in the Hippocampus of a Mouse Model for Down Syndrome during Ageing. *Neurosci. Lett.* **2020**, *714*, 134541.

(21) Fajka-Boja, R.; Hidvégi, M.; Shoenfeld, Y.; Ion, G.; Demydenko, D.; Tömösközi-Farkas, R.; Vizler, C.; Telekes, A.; Resetar, A.; Monostori, E. Fermented Wheat Germ Extract Induces Apoptosis and Downregulation of Major Histocompatibility Complex Class I Proteins in Tumor T and B Cell Lines. *Int. J. Oncol.* **2002**, *20* (3), 563−570.

(22) Marcsek, Z.; Kocsis, Z.; Jakab, M.; Szende, B.; Tompa, A. The Efficacy of Tamoxifen in Estrogen Receptor-Positive Breast Cancer Cells Is Enhanced by a Medical Nutriment. *Cancer Biother. Radiopharm.* **2004**, *19* (6), 746−753.

(23) Comin-Anduix, B.; Boros, L. G.; Marin, S.; Boren, J.; Callol-Massot, C.; Centelles, J. J.; Torres, J. L.; Agell, N.; Bassilian, S.; Cascante, M. Fermented Wheat Germ Extract Inhibits Glycolysis/Pentose Cycle Enzymes and Induces Apoptosis through Poly(ADP-Ribose) Polymerase Activation in Jurkat T-Cell Leukemia Tumor Cells. *J. Biol. Chem.* **2002**, *277* (48), 46408−46414.

https://doi.org/10.1021/acs.jmedchem.5c03226
J. Med. Chem. 2026, 69, 7920−7932

(24) Bullock, A. N.; Debreczeni, J.; Amos, A. L.; Knapp, S.; Turk, B. E. Structure and Substrate Specificity of the Pim-1 Kinase. *J. Biol. Chem.* **2005**, *280* (50), 41675−41682.
(25) Qian, K. C.; Wang, L.; Hickey, E. R.; Studts, J.; Barringer, K.; Peng, C.; Kronkaitis, A.; Li, J.; White, A.; Mische, S.; Farmer, B. Structural Basis of Constitutive Activity and a Unique Nucleotide Binding Mode of Human Pim-1 Kinase. *J. Biol. Chem.* **2005**, *280* (7), 6130−6137.
(26) Bullock, A. N.; Russo, S.; Amos, A.; Pagano, N.; Bregman, H.; Debreczeni, J. E.; Lee, W. H.; Delft, F.; Meggers, E.; Knapp, S. Crystal Structure of the PIM2 Kinase in Complex with an Organoruthenium Inhibitor. *PLoS One* **2009**, *4* (10), No. e7112.
(27) Qian, K. C.; Studts, J.; Wang, L.; Barringer, K.; Kronkaitis, A.; Peng, C.; Baptiste, A.; LaFrance, R.; Mische, S.; Farmer, B. Expression, Purification, Crystallization and Preliminary Crystallographic Analysis of Human Pim-1 Kinase. *Acta Crystallogr., Sect. F: Struct. Biol. Cryst. Commun.* **2005**, *61* (1), 96−99.
(28) Razmazma, H.; Ebrahimi, A.; Hashemi, M. Structural Insights for Rational Design of New PIM-1 Kinase Inhibitors Based on 3,5-Disubstituted Indole Derivatives: An Integrative Computational Approach. *Comput. Biol. Med.* **2020**, *118*, 103641.
(29) Bogusz, J.; Zrubek, K.; Rembacz, K. P.; Grudnik, P.; Golik, P.; Romanowska, M.; Wladyka, B.; Dubin, G. Structural Analysis of PIM1 Kinase Complexes with ATP-Competitive Inhibitors. *Sci. Rep.* **2017**, *7* (1), 13399.
(30) Sever, R.; Brugge, J. S. Signal Transduction in Cancer. *Cold Spring Harb. Perspect. Med.* **2015**, *5* (4), a006098.
(31) Bhullar, K. S.; Lagarón, N. O.; McGowan, E. M.; Parmar, I.; Jha, A.; Hubbard, B. P.; Rupasinghe, H. P. V. Kinase-Targeted Cancer Therapies: Progress, Challenges and Future Directions. *Mol. Cancer* **2018**, *17* (1), 48.
(32) Bachmann, M.; Hennemann, H.; Xing, P. X.; Hoffmann, I.; Möröy, T. The Oncogenic Serine/Threonine Kinase Pim-1 Phosphorylates and Inhibits the Activity of Cdc25C-Associated Kinase 1 (C-TAK1): A NOVEL ROLE FOR Pim-1 AT THE G $_2$/M CELL CYCLE CHECKPOINT. *J. Biol. Chem.* **2004**, *279* (46), 48319−48328.
(33) Winn, L. M.; Lei, W.; Ness, S. A. Pim-1 Phosphorylates the DNA Binding Domain of c-Myb. *Cell Cycle* **2003**, *2* (3), 257−261.
(34) Rainio, E.-M.; Sandholm, J.; Koskinen, P. J. Cutting Edge: Transcriptional Activity of NFATc1 Is Enhanced by the Pim-1 Kinase. *J. Immunol.* **2002**, *168* (4), 1524−1527.
(35) Wang, J.; Kim, J.; Roh, M.; Franco, O. E.; Hayward, S. W.; Wills, M. L.; Abdulkadir, S. A. Pim1 Kinase Synergizes with C-MYC to Induce Advanced Prostate Carcinoma. *Oncogene* **2010**, *29* (17), 2477−2487.
(36) Fox, C. J.; Hammerman, P. S.; Cinalli, R. M.; Master, S. R.; Chodosh, L. A.; Thompson, C. B. The Serine/Threonine Kinase Pim-2 Is a Transcriptionally Regulated Apoptotic Inhibitor. *Genes Dev.* **2003**, *17* (15), 1841−1854.
(37) Koike, N.; Maita, H.; Taira, T.; Ariga, H.; Iguchi-Ariga, S. M. M. Identification of Heterochromatin Protein 1 (HP1) as a Phosphorylation Target by Pim-1 Kinase and the Effect of Phosphorylation on the Transcriptional Repression Function of HP1 [1]. *FEBS Lett.* **2000**, *467* (1), 17−21.
(38) Leverson, J. D.; Koskinen, P. J.; Orrico, F. C.; Rainio, E. M.; Jalkanen, K. J.; Dash, A. B.; Eisenman, R. N.; Ness, S. A. Pim-1 Kinase and P100 Cooperate to Enhance c-Myb Activity. *Mol. Cell* **1998**, *2* (4), 417−425.
(39) Mochizuki, T.; Kitanaka, C.; Noguchi, K.; Muramatsu, T.; Asai, A.; Kuchino, Y. Physical and Functional Interactions between Pim-1 Kinase and Cdc25A Phosphatase: IMPLICATIONS FOR THE Pim-1-MEDIATED ACTIVATION OF THE c-Myc SIGNALING PATHWAY. *J. Biol. Chem.* **1999**, *274* (26), 18659−18666.
(40) Wang, Z.; Bhattacharya, N.; Mixter, P. F.; Wei, W.; Sedivy, J.; Magnuson, N. S. Phosphorylation of the Cell Cycle Inhibitor p21Cip1/WAF1 by Pim-1 Kinase. *Biochim. Biophys. Acta Gen. Subj.* **2002**, *1593* (1), 45−55.
(41) Mukaida, N.; Wang, Y.-Y.; Li, Y.-Y. Roles of Pim-3, a Novel Survival Kinase, in Tumorigenesis. *Cancer Sci.* **2011**, *102* (8), 1437−1442.
(42) Xu, D.; Cobb, M. G.; Gavilano, L.; Witherspoon, S. M.; Williams, D.; White, C. D.; Taverna, P.; Bednarski, B. K.; Kim, H. J.; Baldwin, A. S.; Baines, A. T. Inhibition of Oncogenic Pim-3 Kinase Modulates Transformed Growth and Chemosensitizes Pancreatic Cancer Cells to Gemcitabine. *Cancer Biol. Ther.* **2013**, *14* (6), 492−501.
(43) Abbassi, R.; Johns, T. G.; Kassiou, M.; Munoz, L. DYRK1A in Neurodegeneration and Cancer: Molecular Basis and Clinical Implications. *Pharmacol. Ther.* **2015**, *151*, 87−98.
(44) Becker, W.; Soppa, U.; Tejedor, F. J. DYRK1A: A Potential Drug Target for Multiple Down Syndrome Neuropathologies. *CNS Neurol. Disord.: Drug Targets* **2014**, *13* (1), 26−33.
(45) Demuro, S.; Di Martino, R. M. C.; Ortega, J. A.; Cavalli, A. GSK-3β, FYN, and DYRK1A: Master Regulators in Neurodegenerative Pathways. *Int. J. Mol. Sci.* **2021**, *22* (16), 9098.
(46) Aranda, S.; Laguna, A.; Luna, S. d. l. DYRK Family of Protein Kinases: Evolutionary Relationships, Biochemical Properties, and Functional Roles. *FASEB J.* **2011**, *25* (2), 449−462.
(47) Asati, V.; Mahapatra, D. K.; Bharti, S. K. PIM Kinase Inhibitors: Structural and Pharmacological Perspectives. *Eur. J. Med. Chem.* **2019**, *172*, 95−108.
(48) Hastie, C. J.; McLauchlan, H. J.; Cohen, P. Assay of Protein Kinases Using Radiolabeled ATP: A Protocol. *Nat. Protoc.* **2006**, *1* (2), 968−971.
(49) Vonrhein, C.; Flensburg, C.; Keller, P.; Sharff, A.; Smart, O.; Paciorek, W.; Womack, T.; Bricogne, G. Data Processing and Analysis with the autoPROC Toolbox. *Acta Crystallogr., Sect. D: Biol. Crystallogr.* **2011**, *67* (4), 293−302.
(50) McCoy, A. J.; Grosse-Kunstleve, R. W.; Adams, P. D.; Winn, M. D.; Storoni, L. C.; Read, R. J. *Phaser* Crystallographic Software. *J. Appl. Crystallogr.* **2007**, *40* (4), 658−674.
(51) Emsley, P.; Lohkamp, B.; Scott, W. G.; Cowtan, K. Features and Development of *Coot*. *Acta Crystallogr., Sect. D: Biol. Crystallogr.* **2010**, *66* (4), 486−501.
(52) Adams, P. D.; Afonine, P. V.; Bunkóczi, G.; Chen, V. B.; Davis, I. W.; Echols, N.; Headd, J. J.; Hung, L.-W.; Kapral, G. J.; Grosse-Kunstleve, R. W.; McCoy, A. J.; Moriarty, N. W.; Oeffner, R.; Read, R. J.; Richardson, D. C.; Richardson, J. S.; Terwilliger, T. C.; Zwart, P. H. *PHENIX*: A Comprehensive Python-Based System for Macromolecular Structure Solution. *Acta Crystallogr., Sect. D: Biol. Crystallogr.* **2010**, *66* (2), 213−221.
(53) Chen, V. B.; Arendall, W. B.; Headd, J. J.; Keedy, D. A.; Immormino, R. M.; Kapral, G. J.; Murray, L. W.; Richardson, J. S.; Richardson, D. C. *MolProbity*: All-Atom Structure Validation for Macromolecular Crystallography. *Acta Crystallogr., Sect. D: Biol. Crystallogr.* **2010**, *66* (1), 12−21.

https://doi.org/10.1021/acs.jmedchem.5c03226
J. Med. Chem. 2026, 69, 7920−7932